

# PROCEEDINGS OF SPIE

[SPIDigitalLibrary.org/conference-proceedings-of-spie](https://SPIDigitalLibrary.org/conference-proceedings-of-spie)

## Dual-wavelength photoacoustic imaging for guidance of hysterectomy procedures

Wiacek, Alycen, Wang, Karen, Wu, Harold, Bell, Muyinatu A. Lediju

Alycen Wiacek, Karen C. Wang, Harold Wu, Muyinatu A. Lediju Bell, "Dual-wavelength photoacoustic imaging for guidance of hysterectomy procedures," Proc. SPIE 11229, Advanced Biomedical and Clinical Diagnostic and Surgical Guidance Systems XVIII, 112291D (21 February 2020); doi: 10.1117/12.2544906

**SPIE.**

Event: SPIE BiOS, 2020, San Francisco, California, United States

# Dual-wavelength photoacoustic imaging for guidance of hysterectomy procedures

Alycen Wiacek<sup>a,\*</sup>, Karen C. Wang<sup>b</sup>, Harold Wu<sup>b</sup>, and Muyinatu A. Lediju Bell<sup>a,c,d</sup>

<sup>a</sup>Department of Electrical and Computer Engineering, Johns Hopkins University, USA

<sup>b</sup>Department of Gynecology and Obstetrics, Johns Hopkins Medicine, USA

<sup>c</sup>Department of Biomedical Engineering, Johns Hopkins University, USA

<sup>d</sup>Department of Computer Science, Johns Hopkins University, USA

## ABSTRACT

Gynecologic surgery accounts for 75% of all intraoperative injuries to the ureters, due to the close proximity of the ureter to the uterine artery. We propose dual-wavelength photoacoustic imaging in order to distinguish the ureter from the uterine artery, identify the position of the surgical tool in proximity to these critical structures, and assist with guidance of hysterectomy procedures. Experiments were performed in a pilot human cadaver study and a dual-wavelength approach was introduced to visualize the uterine artery and a ureter filled with urine and methylene blue. The ureter location was identified with low contrast at a wavelength of 750 nm and higher contrast at a wavelength of 690 nm, resulting in a 5.8 dB contrast difference in photoacoustic signals from the ureter at these two different wavelengths. The uterine artery was identified at laser wavelengths of both 690 nm and 750 nm, with similarly high contrasts of 17.4 dB and 16.0 dB, respectively. By using a dual-wavelength display, both the ureter and the uterine artery were identified and their position was estimated in the photoacoustic image. The proximity of a surgical tool tip to the ureter was additionally estimated based on the information provided in the dual-wavelength photoacoustic display and mapped to an auditory signal. This auditory information can be provided as either an alternative or an addition to photoacoustic images that inform surgeons of the risk of injury. Results highlight the promise of dual-wavelength photoacoustic imaging to achieve our ultimate goal of avoiding accidental ureteral injuries during hysterectomies and possibly other similar gynecologic surgeries and procedures.

## 1. INTRODUCTION

Hysterectomy, the surgical removal of the uterus, is the most common nonobstetric surgical procedure for women performed in the United States, with over 600,000 procedures performed each year.<sup>1</sup> A hysterectomy requires the transection or cauterization of the uterine arteries that lie within millimeters of the ureter.<sup>2</sup> The incidences of ureteral injury range from 0.4% - 2.5%<sup>3,4</sup> for non-malignant conditions, which translates to as many as 15,000 injuries per year for these patients in the United States. When discovered intraoperatively, these injuries can be addressed immediately to avoid serious complications and post operative sequelae. For example, Blackwell *et al.*<sup>4</sup> reported that 62% of ureteral injuries went unrecognized during hysterectomy procedures, resulting in 67% of patients readmitted to hospitals, as well as life threatening complications such as sepsis and acute renal insufficiency in 16.9% and 28% of patients, respectively.

Although our focus is hysterectomy, a similar risk of accidental ureteral injury exists for other gynecological procedures, such as oophorectomy, cesarean section, and presacral neurectomy.<sup>3</sup> Due to the close proximity to the ureter, gynecologic surgery accounts for 75% of all intraoperative injuries to the ureters.<sup>5</sup> However, 50-70% of ureteral injuries are undetected,<sup>6</sup> leading to additional surgeries, prolonged recovery, renal insufficiency, and patient death.

One approach to avoid ureteral injury is to use intravenous fluorescent dyes such as methylene blue,<sup>7,8</sup> sodium fluorescein, or investigational dyes<sup>9</sup> that respond to specific wavelengths of light.<sup>10</sup> However, this approach requires specialized endoscopic equipment and is more challenging in patients with endometriosis, pelvic malignancies, or extensive scar tissue from previous surgeries, where the ureter is difficult to find beneath tissue. In addition, this approach does not provide information about the proximity of the surgical tool to the ureter.

Previous work demonstrated the feasibility of photoacoustic imaging of urine mixed with methylene blue housed in tubing during a series of experiments with and without *ex vivo* tissue.<sup>11</sup> However, artifacts from the plastic tubing resulted in challenges with isolating the photoacoustic signals from the methylene blue. We hypothesized that similar results demonstrating the feasibility of ureter visualization with photoacoustic imaging could be obtained in the absence of tubing when imaging human cadaver ureters (prior to translating the proposed technology to human patients).

The work presented in this paper builds on our initial success with phantom experiments<sup>11,12</sup> and demonstrates the proposed photoacoustic imaging system in a pilot human cadaver study. In general, to perform photoacoustic imaging, targets of interest (e.g., a ureter containing urine mixed with methylene blue) are illuminated using optical energy, which is subsequently absorbed by the targets, resulting in the generation of a mechanical pressure wave that can be sensed with a conventional ultrasound transducer.<sup>13</sup> More specifically, to perform photoacoustic-guided hysterectomy to avoid the ureters during surgery, an ultrasound transducer can be placed for transvaginal sound reception, and the transmitted light can be tuned to wavelengths near 609 nm or 668 nm, which represent the optical absorption peaks of methylene blue. The photoacoustic imaging system can additionally visualize the nearby uterine arteries<sup>12</sup> and surgical tool tips that can be attached to the light source,<sup>14</sup> due to the optical absorption properties of hemoglobin and metal, respectively. Combining the optical absorption properties of hemoglobin, methylene blue, and metal, we propose dual-wavelength photoacoustic imaging for intraoperative visualization of the ureter, the uterine artery, and the surgical tool in order estimate the position of the ureter relative to the surgical tool tip for intraoperative guidance of hysterectomies.

## 2. METHODS

### 2.1 Experimental Setup

The torso of a human cadaver was opened with a midline vertical incision. The ureter and distal portion of the uterine artery were dissected and sutured at the distal end. The uterine artery was injected with whole human blood, and the ureter was filled with urine mixed to a concentration of 400  $\mu\text{M}$  with methylene blue. The artery and ureter were then sutured at the proximal end. A Phocus Mobile laser (Opotek, Inc., Carlsbad, CA) operating at wavelengths from 690 nm to 800 nm was coupled to a 5 mm-diameter fiber bundle emitting an average energy of 45.5 mJ per pulse. This setup was used to illuminate the ureter and uterine artery. Co-registered ultrasound and photoacoustic data were acquired using an Alpinion ECUBE12R research ultrasound scanner (Alpinion, Seoul, Korea), connected to an Alpinion EC3-10 transvaginal ultrasound probe, which had a center frequency of 7.5 MHz and an ultrasound transmit frequency of 7.1 MHz.

Ultrasound and photoacoustic channel data were acquired both with and without a laparoscopic grasper tool tip (Autosuture Endo Grasp, Medtronic, Fridley, MN) in the imaging plane. When the laparoscopic tool was in the imaging plane, it was navigated between the ureter and uterine artery. First, the tool touched the ureter, then it was swept the direction of the uterine artery, and finally it touched the uterine artery. This motion was then reversed and repeated for approximately 3 seconds. Co-registered ultrasound and photoacoustic videos of this motion were acquired with the goals of visualizing differences in the photoacoustic signals and exploring possible surgical display methods.

### 2.2 Data Acquisition and Analysis

Standard delay-and-sum (DAS) beamforming was used to create ultrasound images. Both DAS beamforming and short-lag spatial coherence (SLSC) beamforming were applied to create photoacoustic images. SLSC beamforming was originally proposed for ultrasound imaging and has been shown to significantly reduce acoustic clutter and increase the contrast of photoacoustic images.<sup>15,16</sup> SLSC beamforming was implemented when incoherent noise caused difficulty with the interpretation of DAS images.

To implement SLSC beamforming, receive delays were applied to the raw photoacoustic channel data. The normalized cross-correlation between signals received by equally spaced elements (i.e., spatial lags) was then calculated with an axial kernel size,  $k = n_2 - n_1$ , that is equivalent to one wavelength<sup>17</sup> as follows:

$$\hat{R}(m) = \frac{1}{N - m} \sum_{i=1}^{N-m} \frac{\sum_{n=n_1}^{n_2} s_i(n) s_{i+m}(n)}{\sqrt{\sum_{n=n_1}^{n_2} s_i^2(n) \sum_{n=n_1}^{n_2} s_{i+m}^2(n)}} \quad (1)$$

where  $N$  is the number of elements in the transducer,  $m$  is the spatial lag in units of number of elements,  $s_i(n)$  is a time-delayed, zero-mean signal received at element  $i$  from depth  $n$ . The resulting spatial coherence function was then summed up to a specific short-lag value,  $M$ , yielding the value of the SLSC image pixel. This process was repeated for each lateral and axial position in the image.

To assess the visibility of signals in beamformed photoacoustic images, the laser wavelength was tuned from 690 to 800 nm, and contrast was measured as a function of wavelength as follows:

$$\text{Contrast} = 20 \log_{10} \left( \frac{S_i}{S_o} \right) \quad (2)$$

where  $S_i$  and  $S_o$  are the means of signals within regions of interest (ROIs) inside and outside of a target, respectively. The blood ROI was selected as a 1.5 mm circle surrounding the brightest pixel at 750 nm (i.e., the ideal optical absorption peak of deoxygenated hemoglobin). Subtracting the region in the photoacoustic image already identified as blood, the ureter ROI was selected as the 1.5 mm radius surrounding the brightest pixel in the image at 690 nm (i.e., the nearest available wavelength to the 668 nm optical absorption peak of methylene blue).

### 2.3 Custom Display and Mapping Methods

In addition to individually displaying each acquired photoacoustic image, normalized by the brightest pixel in the image, two custom methods were implemented in efforts to explore feasible approaches to display information of interest to surgeons for guidance during hysterectomies. First, in order to leverage the maximum contrast differences in the photoacoustic signals from methylene blue and deoxygenated hemoglobin, a custom dual-wavelength display was created. The image created with the wavelength that produced the maximum contrast difference between photoacoustic signals from methylene blue and hemoglobin (i.e., 750 nm) was displayed on a red color map, and the image created with the wavelength that produced the maximum methylene blue image contrast (i.e., 690 nm) was displayed on a blue color map. Each image was individually normalized by its brightest pixel and displayed with a dynamic range that enhanced signal visualization, then both images were overlaid on the grayscale ultrasound image.

The second custom method mapped the measured distance between the laparoscopic tool and ureter to sound, using the data acquired during the tool motion experiment described in Section 2.1 (in addition to using the visual feedback of the dual-wavelength display described above). To accomplish the auditory mapping, the tool was selected as the region surrounding the brightest pixel in the image (as metal has the highest optical absorption compared to hemoglobin and methylene blue<sup>18</sup>). The positions of the ureter was selected based on its photoacoustic signal appearance at 690 nm and 750 nm wavelengths. The Euclidean distance between the tool tip and the ureter was then calculated. When the absolute distance between the tool and the ureter fell below a given threshold (i.e., 5 mm for the cadaver study), an audible beeping ensued, starting at a frequency of 3.5 kHz and increasing to 5.5 kHz if the tool came in contact with the ureter. In addition, a dual-wavelength display was created to visualize the tool motion, using the color map of red for blood, blue for urine, and green for the surgical tool tip. Each identified region of interest was normalized by its brightest pixel and displayed with a dynamic range that enhanced signal visualization.

## 3. RESULTS

### 3.1 Individual Photoacoustic Images

Fig. 1 shows the results from the individual photoacoustic images used to select wavelengths for the dual-wavelength photoacoustic display. Figs. 1(a) and (b) show the photoacoustic image created using DAS beamforming overlaid on the ultrasound image at 690 nm and 750 nm wavelength, respectively. Qualitatively, the signal from the urine and methylene blue is present at 690 nm, as seen during previous phantom studies,<sup>11</sup> and then reduces in amplitude at 750 nm. These trends are quantified in Fig. 1(c), which shows that the contrast of urine mixed with methylene blue is highest at 690 nm wavelength (i.e., 17.3 dB), and drops to a contrast of 11.5 dB at 750 nm wavelength, resulting in a 5.8 dB contrast difference between these two wavelengths. The contrast of blood remains relatively high across wavelengths, measuring 17.4 dB and 16.0 dB at 690 nm and 750 nm wavelengths, respectively. The contrast difference between urine mixed with methylene blue and blood was 0.1 dB at 690 nm wavelength and 4.5 dB at 750 nm wavelength.

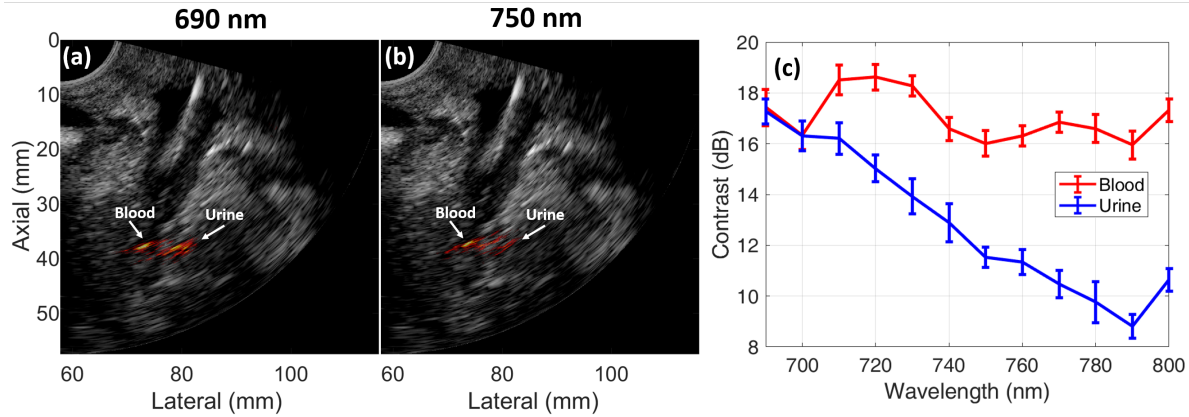


Figure 1. Example DAS photoacoustic images from the human cadaver study, obtained with (a) 690 nm and (b) 750 nm laser wavelengths overlaid on co-registered ultrasound images. (c) Contrast measurements as a function of wavelength.

### 3.2 Dual-Wavelength Display

Fig. 2 shows individual SLSC photoacoustic images acquired with 690 nm and 750 nm wavelengths, followed by the custom dual-wavelength image. The mostly blue signal (i.e., associated with 690 nm wavelength results) represents the urine, and the mostly red signal (i.e., associated with 750 nm wavelength results) represents the blood. These photoacoustic images were formed using SLSC beamforming in order to remove the incoherent noise that was present in the DAS images (see Fig. 1 for comparison) and to clarify the position of each structure based on the brightest pixel in the SLSC photoacoustic image.

Because the photoacoustic image obtained with 690 nm is displayed in blue, the photoacoustic signal from the methylene blue stands out compared to the photoacoustic signal at 750 nm, where blood dominates. Note that it is difficult to differentiate blood signal obtained with 690 nm wavelength in the dual wavelength image because the blood signal obtained with 690 nm wavelength is overlapped by the blood signal obtained with 750 nm wavelength. Nonetheless, the differences in optical absorption at each wavelength allows the ureter to be differentiated from the uterine artery by switching between these two wavelengths.

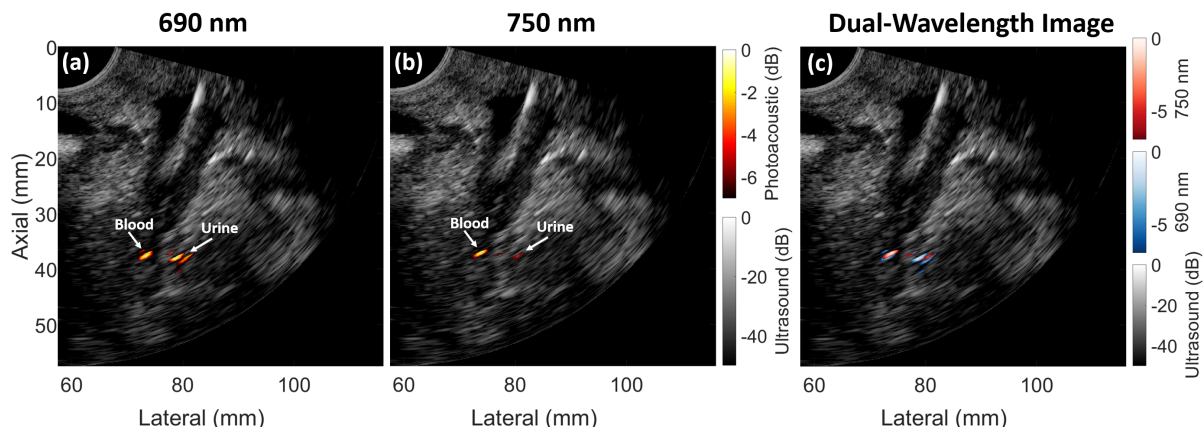


Figure 2. Example SLSC photoacoustic images from the human cadaver study, obtained with (a) 690 nm and (b) 750 nm laser wavelengths overlaid on co-registered ultrasound images. (c) The corresponding dual-wavelength photoacoustic image display showing the 690 nm and 750 nm wavelength results in blue and red, respectively, overlaid on co-registered ultrasound images.

### 3.3 Auditory Mapping

Fig. 3(a) shows an example dual-wavelength photoacoustic image that includes the surgical tool. This display was used to estimate the tool position and map this distance information to an auditory signal. The photoacoustic signal from blood is shown in red, the photoacoustic signal from urine and methylene blue is shown in blue, and the photoacoustic signal from the laparoscopic tool is shown in green. These photoacoustic images were created with SLSC beamforming in order to remove incoherent noise in the DAS image and improve signal visibility. The box surrounding each signal represents the detected position according to the algorithm (i.e., the uterine artery in red, the ureter in blue, and the laparoscopic tool in green). The measured Euclidean distance between the tool and the ureter was displayed as a text overlay on the image (i.e., 4.63 mm in Fig. 3(a)).

Fig. 3(b) shows calculated distances as a function of time. When the distance between the laparoscopic tool and the ureter ranged from 0 mm to 5 mm, the frequency of the sound increased, until the tool was touching the ureter. Because the distance was calculated from the center of the ureter, a distance of 2 mm indicates that the tool was touching the edge of the ureter.

Fig. 3(c) shows the resulting audio signal, which was plotted at 1/1000th of the original frequency in order to visually appreciate differences in the audio signal. Although the true audio signal was modulated from 3.5 kHz to 5.5 kHz, these frequencies were too high to appropriately visualize the changes in the signal while keeping the full time axis. Therefore, the modified signal in Fig. 3(c) shows scaled audio signal frequencies ranging 3.5 Hz to 5.5 Hz to allow for visualization of frequency changes as a function of time.

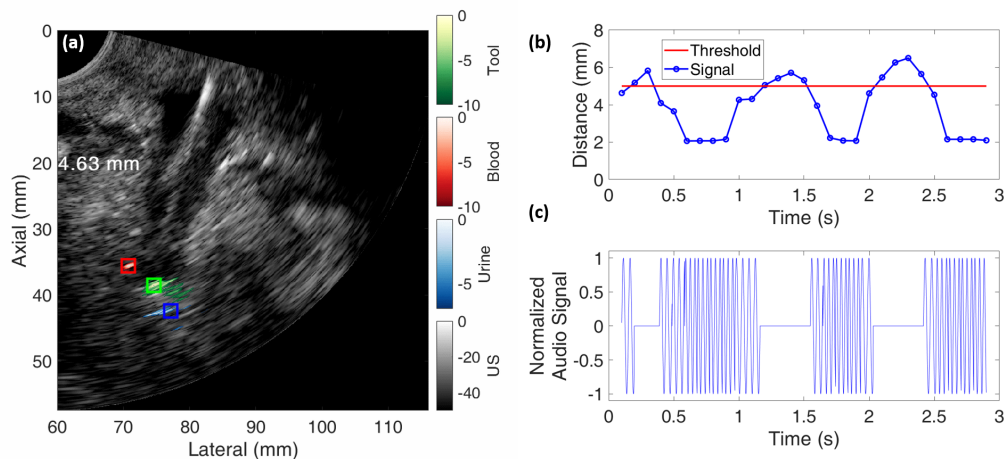


Figure 3. (a) Example dual wavelength photoacoustic image showing the ureter in blue, the tool in green, and the artery in red. (b) Calculated distance as a function of time. (c) Mapped audio signal scaled to 1/1000th of the audio frequency in order to visually appreciate frequency differences.

## 4. DISCUSSION

The results presented in this paper demonstrate the promise of using photoacoustic imaging to guide hysterectomies and successfully overcomes previous challenges with confounding signals from blood- and urine-filled tubes.<sup>11</sup> The replacement of tubing with vessels and ureters in a human cadaver provides confidence that the signals observed in previous tubing-based experiments were associated with blood and methylene blue, considering the similar trends observed in Fig. 1. Specifically, the urine mixed with methylene blue has photoacoustic contrast that decreases with increasing wavelength, and the blood has photoacoustic contrast that is greater than the contrast of the urine mixed with methylene blue at a wavelength of 750 nm.

With this confidence, we can move forward with explorations of methods to convey this useful information to surgeons during *in vivo* studies. For example, we can take advantage of a laser system that is programmed to switch between two wavelengths, as described in previous work for simultaneous nerve and blood visualization.<sup>19</sup> We built on this previous work<sup>19</sup> with development of the dual wavelength display format represented in Fig. 2,

which has the potential to identify the ureter and uterine artery during surgery using two wavelengths of interest (i.e., 690 nm and 750 nm). Considering the high optical absorption of metal, information about the location of a metal surgical tool tip can be added to this dual-wavelength display format, as shown in Fig. 3(a).

In addition to the visual information presented in Figs. 2 and 3(a), the ability to provide auditory feedback based on the same photoacoustic data utilized to make images has additional promise for the proposed approach. With auditory feedback, surgeons would have the option to focus on the surgical field without the additional requirement to observe a monitor displaying photoacoustic images. Future work includes a cadaver study to determine feasibility of the proposed approaches under laparoscopic surgical conditions and an investigation of surgeons' preferences for auditory or visual feedback.

## 5. CONCLUSION

This work is the first to utilize dual-wavelength photoacoustic imaging to estimate the position of the ureter relative to the surgical tool in order to guide hysterectomy procedures. Successful signal differentiation was achieved in a pilot cadaver study that did not require the use of tubing, which was previously shown to confound signals of interest. A contrast difference of 5.8 dB was measured between the photoacoustic signals from the ureter obtained with wavelengths of 690 nm and 750 nm. This contrast difference was sufficient to estimate the ureter position. In addition, we demonstrated that information can be provided as visual or auditory cues for possible surgical guidance. These results are promising for the introduction of dual-wavelength photoacoustic imaging to help differentiate the ureter from the uterine artery, estimate the position of the ureter relative to a surgical tool tip, and ultimately guide hysterectomy procedures to avoid accidental ureteral injuries.

## ACKNOWLEDGMENTS

This work was funded by a Johns Hopkins Discovery Award. Thanks to Michelle Graham for her assistance during the cadaver study.

## REFERENCES

- [1] H. Keshavarz, S. D. Hillis, B. A. Kieke, *et al.*, "Hysterectomy surveillance—united states, 1994–1999," *MMWR CDC Surveill Summ* **51**(SS05), 1–8 (2002).
- [2] P. L. Williams, L. Bannister, M. Berry, *et al.*, "Gray's anatomy: the anatomical basis of medicine and surgery," *Edinburgh: Churchill Livingstone* **38**, 1560 (1995).
- [3] M. Drake and J. Noble, "Ureteric trauma in gynecologic surgery," *International Urogynecology Journal* **9**(2), 108–117 (1998).
- [4] R. H. Blackwell, E. J. Kirshenbaum, A. S. Shah, *et al.*, "Complications of recognized and unrecognized iatrogenic ureteral injury at time of hysterectomy: a population based analysis," *The Journal of Urology* **199**(6), 1540–1545 (2018).
- [5] R. A. Dowling, J. N. Corriere Jr, and C. M. Sandler, "Iatrogenic ureteral injury," *The Journal of Urology* **135**(5), 912–915 (1986).
- [6] S. E. Delacroix Jr and J. Winters, "Urinary tract injuries: recognition and management," *Clinics in Colon and Rectal Surgery* **23**(2), 104 (2010).
- [7] A. Matsui, E. Tanaka, H. S. Choi, *et al.*, "Real-time, near-infrared, fluorescence-guided identification of the ureters using methylene blue," *Surgery* **148**(1), 78–86 (2010).
- [8] F. P. Verbeek, J. R. van der Vorst, B. E. Schaafsma, *et al.*, "Intraoperative near infrared fluorescence guided identification of the ureters using low dose methylene blue: a first in human experience," *The Journal of Urology* **190**(2), 574–579 (2013).
- [9] R. W. Farnam, R. G. Arms, A. H. Klaassen, *et al.*, "Intraoperative ureter visualization using a near-infrared imaging agent," *Journal of Biomedical Optics* **24**(6), 066004 (2019).
- [10] K. Papatla, J. Brown, and K. L. Houck, "Prevention and early identification of urinary tract injury during minimally invasive surgery," *Topics in Obstetrics & Gynecology* **38**(2), 1–7 (2018).

- [11] A. Wiacek, K. C. Wang, and M. A. L. Bell, "Techniques to distinguish the ureter from the uterine artery in photoacoustic-guided hysterectomies," in *Photons Plus Ultrasound: Imaging and Sensing 2019*, **10878**, 108785K, International Society for Optics and Photonics (2019).
- [12] M. Allard, J. Shubert, and M. A. L. Bell, "Feasibility of photoacoustic-guided teleoperated hysterectomies," *Journal of Medical Imaging* **5**(2), 021213 (2018).
- [13] P. Beard, "Biomedical photoacoustic imaging," *Interface Focus* **1**(4), 602 (2011).
- [14] B. Eddins and M. A. L. Bell, "Design of a multifiber light delivery system for photoacoustic-guided surgery," *Journal of Biomedical Optics* **22**(4), 041011 (2017).
- [15] M. A. L. Bell, N. Kuo, D. Y. Song, *et al.*, "Short-lag spatial coherence beamforming of photoacoustic images for enhanced visualization of prostate brachytherapy seeds," *Biomedical Optics Express* **4**(10), 1964–1977 (2013).
- [16] B. Pourebrahimi, S. Yoon, D. Dopsa, *et al.*, "Improving the quality of photoacoustic images using the short-lag spatial coherence imaging technique," in *Photons Plus Ultrasound: Imaging and Sensing 2013*, **8581**, 85813Y, International Society for Optics and Photonics (2013).
- [17] M. A. L. Bell, J. J. Dahl, and G. E. Trahey, "Resolution and brightness characteristics of short-lag spatial coherence (slsc) images," *IEEE Transactions on Ultrasonics, Ferroelectrics, and Frequency Control* **62**(7), 1265–1276 (2015).
- [18] B. Karlsson, C. G. Ribbing, A. Roos, *et al.*, "Optical properties of some metal oxides in solar absorbers," *Physica Scripta* **25**(6A), 826 (1982).
- [19] M. T. Graham, J. Y. Guo, and M. A. L. Bell, "Simultaneous visualization of nerves and blood vessels with multispectral photoacoustic imaging for intraoperative guidance of neurosurgeries," in *Advanced Biomedical and Clinical Diagnostic and Surgical Guidance Systems XVII*, **10868**, 108680R, International Society for Optics and Photonics (2019).